Study of Combustion Processes of Single-Perforated Stick Propellants

J. M. Char* and K. K. Kuo†
Pennsylvania State University, University Park, Pennsylvania

This paper addresses flame-spreading, combustion, and grain-rupture processes associated with unslotted single-perforated stick propellants, both theoretically and experimentally. A coupled finite-difference and finite-element code was developed for solving the property variations in gas- and solid-phase regions. Tests were conducted using a windowed chamber for observation of the transient combustion and fracture phenomena. Test data indicate that higher pressurization rate causes earlier propellant ignition and faster flame-spreading rate. Critical pressure differential across the propellant web for grain rupture was found to increase monotonically with the internal pressurization rate. Recovered propellant samples showed that longitudinal slits were formed at low pressurization rates, while at rapid pressurization rates (higher than 3.5 GPa/s), the grains shattered into many small pieces. Depending upon the internal pressurization rates, scanning electron microscope microstructure of fractured surfaces of recovered grains exhibited ductile-tensile, ductile-shear, or brittle-cleavage phenomena. Calculated results, in agreement with experimental data, provide reasonable physical interpretation of the complicated and coupled combustion/structural mechanics problem.

Introduction

INTEREST in the use of single-perforated long stick-propellant charges in large-caliber gun systems continues to grow. Although the advantages of stick propellants over granular propellants for high-performance large-caliber gun systems have been noted, the true mechanism for improved performance has not yet been totally identified. Numerous studies conducted by a number of investigators[1-11] indicate that one of the major advantages of stick propellants over conventional, randomly packed grains is that a larger mass of propellant can be loaded into the same volume, resulting in an increase in gun performance and flexibility of charge design. Since loading density can be higher when stick propellants are used, this configuration is preferable for low-vulnerability-ammunition (LOVA) propellants, which require increased mass of propellant charge to produce equivalent performance. It has been demonstrated further that flow resistance through the charge is lower for stick propellants, thus enabling a faster and more reproducible flame-spreading rate over the charge; this also reduces undesirable high-pressure gradients and severe pressure waves in gun systems. Consequently, it is possible to achieve higher ballistic reproducibility with stick propellants.

Robbins and Horst[1] reported on a mechanism to improve gun performance using stick-propellant charges. Stick propellants have larger mass and, hence, less mobility than granular propellants. They usually burn in the relatively high-pressure zone near the breech end. They can also be loaded more easily than bag charges, since stick propellants can be prepackaged in various desired dimensions. However, although there is considerable evidence to support the fact that higher muzzle velocity and improved overall gun performance can be achieved when stick propellants replace conventional granular propellants, the mechanism for improved performance is not yet fully understood.

In the past, partial phenomena of single-stick propellant combustion and fracture have been studied by several research groups. The flow resistance in a stick-propellant charge was measured by Robbins et al.[8] A lumped-parameter modeling of burning inside the perforation and on the exterior surfaces of unslotted stick propellant was conducted by Robbins and Horst.[2] They found that even with a unity discharge coefficient, pressure differentials across the web exceed the bursting strength by an order of magnitude. Robbins and Horst[4] also conducted experiments at constant external pressure of 1 atm. Progressive-interior surface burning caused by the locally increased pressure was noted in fractured grain fragments recovered from tests. Athavale et al.[7] observed rupture phenomena under various internal pressurization rates. The critical pressure for dynamic fracture was found to be an order of magnitude higher than that at quasisteady conditions. A theoretical model was also formulated by Athavale et al.[7] based on a one-dimensional transient gas-phase analysis coupled with axisymmetric dynamic structural analysis for the solid propellant. However, no direct comparison of calculated results with experimental data was conducted.

The focus of this continued research is to achieve a better understanding of the complicated interaction of flame spreading, combustion, grain deformation, and rupture inside the perforation region of a stick propellant by 1) obtaining more detailed flame-spreading and grain-fracture phenomena, 2) comparing theoretical predictions with experimental data, and 3) determining the applicability of the theoretical model and computer code in predicting this complicated event.

Theoretical Approach

As previously mentioned, a comprehensive theoretical model for predicting the flame-spreading, combustion, grain deformation, and fracture processes of an unslotted single-perforated stick propellant was formulated by Athavale et al.[7] A schematic diagram of the physical model for combustion and fracture of a single-perforated unslotted stick-propellant grain is shown in Fig. 1. In the theoretical formulation, three regions are considered: 1) internal perforation region; 2) solid propellant region; and 3) external region. A finite-difference scheme is used to solve the flow properties in the gas phase and a finite-element method is used in the solid-phase analysis. The following are several special features of the model.

1) A transient, one-dimensional analysis was adopted for predicting combustion properties in the gas phase. Real-gas effect, erosive-burning formula, and special treatment on the boundary conditions were considered in the model.

Presented as Paper 87-2029 at the AIAA/SAE/ASME/ASEE 23rd Joint Propulsion Conference, San Diego, CA, June 29-July 2, 1987; received Sept. 4, 1987; revision received June 8, 1988.

*Ph.D. Candidate.
†Distinguished Alumni Professor of Mechanical Engineering. Associate Fellow AIAA.

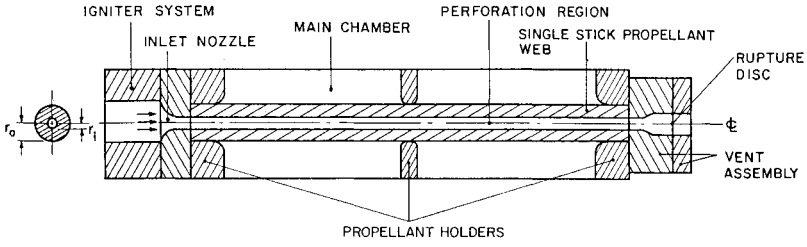

Fig. 1 Schematic diagram of the physical model for combustion and fracture of a single-perforated unslotted stick-propellant grain.

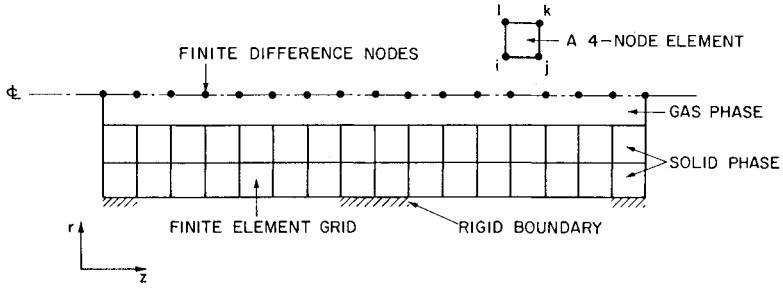

Fig. 2 Structure of finite-difference and finite-element nodes (the total numbers of nodes and elements are reduced for clarity).

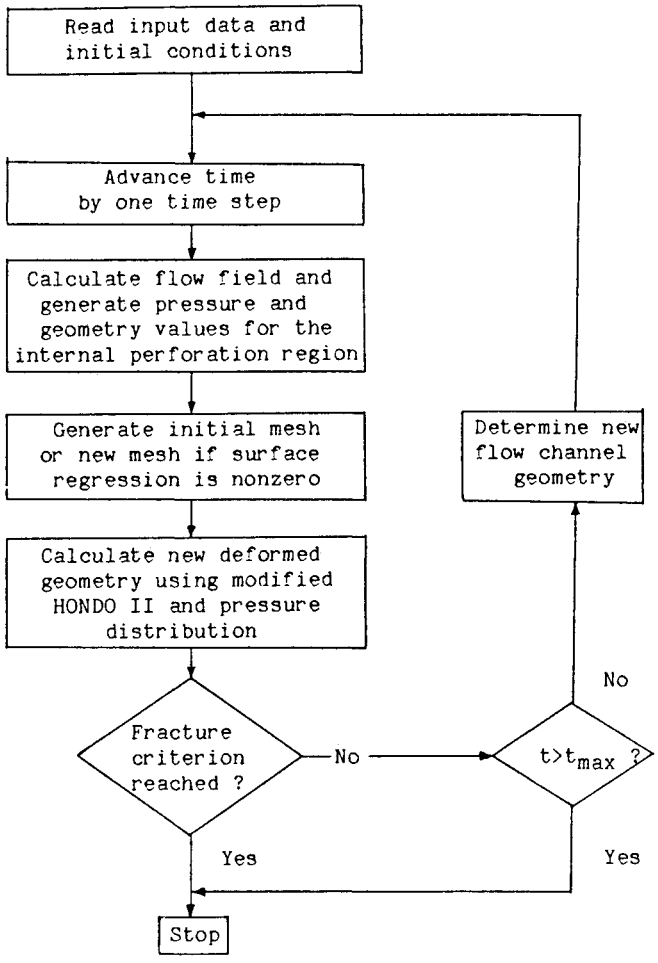

Fig. 3 Overall computation procedure.

2) A transient, two-dimensional structural analysis for calculating propellant grain deformation, stress distribution, and fracture was applied to the solid phase. The NOSOL-363 propellant was treated as a viscoelastic material in shear and elastic material in bulk deformation under dynamic loading conditions. Transient structural mechanics analysis is essential, since experimental evidence[7] has indicated the strong dependence of critical rupture pressure on pressurization rates. The well-developed HONDO-II code[12] was utilized for the calculation.

3) Since NOSOL-363 propellants used in this investigation are translucent, subsurface radiation absorption has been considered. The theoretical formulation adopts a two-flux model in the treatment of radiative heat fluxes.

4) A coupled subprogram was developed to combine the combustion process with the grain dynamic deformation. Propellant grain regression caused by combustion and deformation due to dynamic loading was calculated at each time step. The instantaneous web thickness and surface location of the internal perforation were then used to generate new flow-channel geometry.

Numerical Approach

Combustion Code

A generalized implicit scheme, based on central difference in spanwise derivatives, was chosen to solve the governing equations numerically. A weighting parameter θ is used to control the degree of implicitness of the numerical scheme. The value of θ is 0.5 for the Crank-Nicolson scheme, and a value of 0.6 is used in the numerical simulation for the gas phase.

Solid-Mechanics Code

In the HONDO-II code, the Galerkin form of the finite-element method is used to generate the spacial discretization.[12] This may also be viewed as a use of the principle of virtual work. An arbitrary quadrilateral mesh was adopted. The motion of the boundary of elements is assumed to vary bilinearly over the element using isoparametric coordinates. An element-by-element process is used to generate the equations of motion for all nodes. The resulting simultaneous equations in time are integrated using the central-difference expression for velocity and displacement. Since a diagonal mass matrix is used, the scheme is explicit and, therefore, computationally very fast per time step. This integration procedure, which is conditionally stable with respect to time-step size, provides a very simple, reliable, continuous monitor of the step-size used in the program.

Overall Computation Procedure

The structure of finite-difference grids with finite-element nodes is shown in Fig. 2. The overall flowchart and detailed calculation procedure are shown in Fig. 3. Calculation of the mechanical behavior of the solid propellant is performed by the subprogram, HONDO-II, which is coupled to the finite-difference program. To reduce computational costs, HONDO-II is called after each five time-step calculations of gas-phase properties. This procedure has a negligible effect on the accuracy of the calculated results, since mechanical deforma-

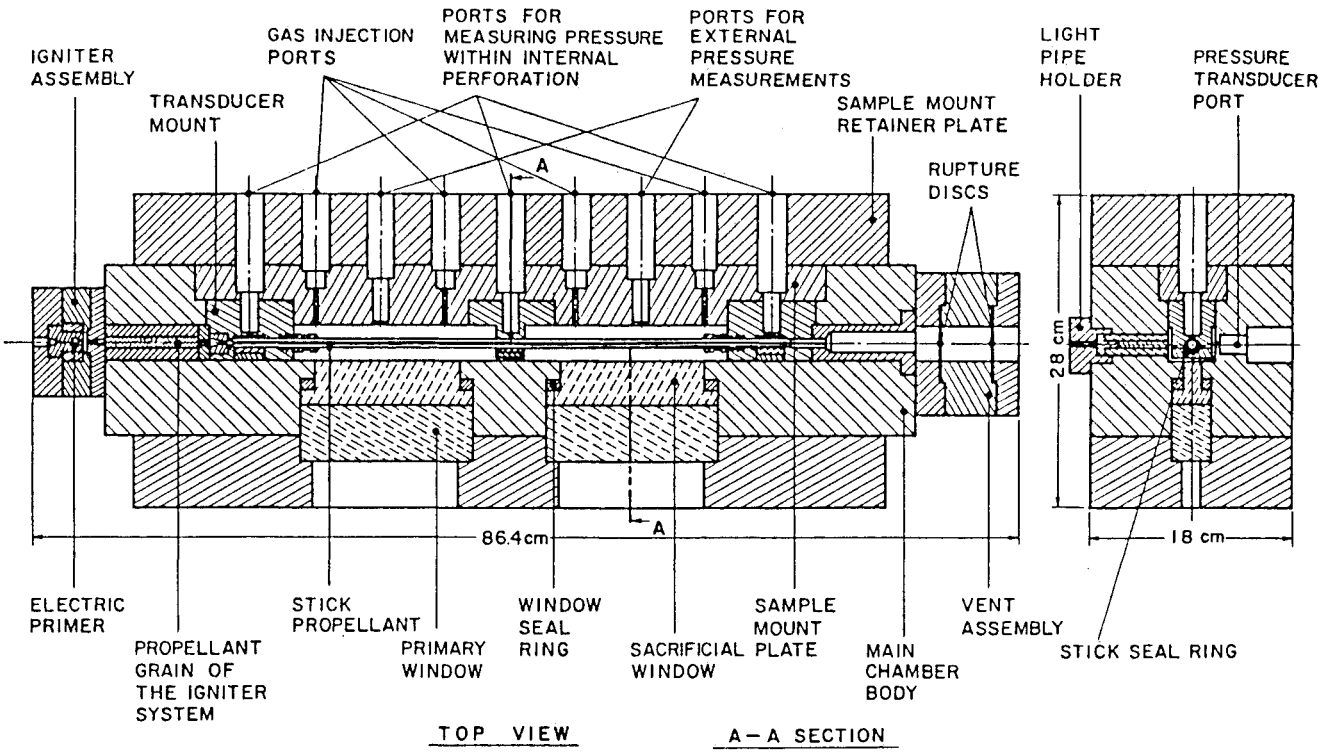

Fig. 4 Schematic diagram of test-rig assembly for studying combustion and fracture of a single-perforated stick propellant.

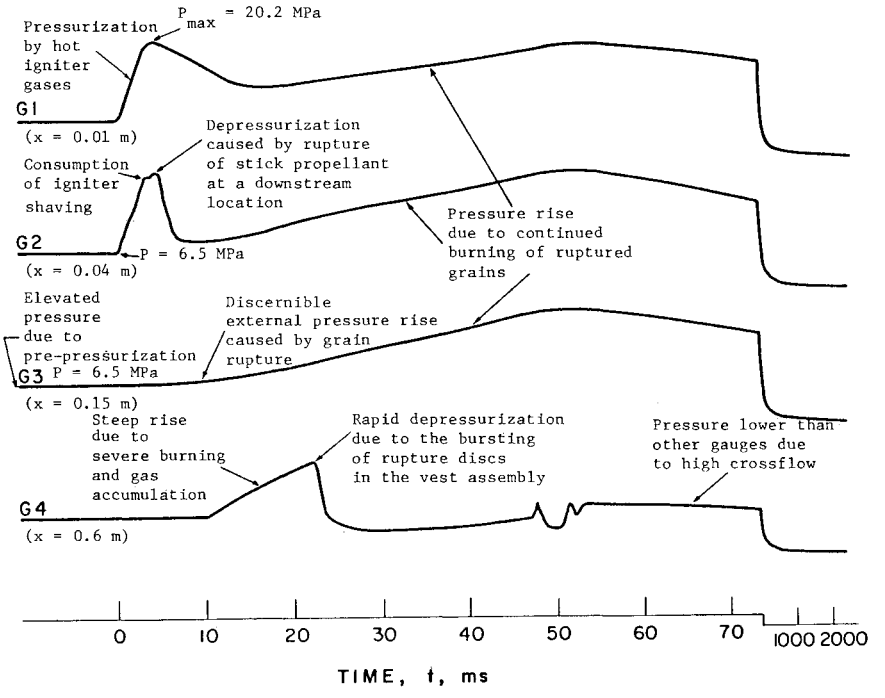

Fig. 5 Typical set of pressure-time traces in the combustion and fracture of a single-perforated NOSOL-363 stick propellant (test no. DADP-18).

tion within each time step for the gas-phase calculation (2 μs) is extremely small. The amount of mechanical deformation is then divided into five increments and distributed to the five time steps in the next gas-phase calculations.

Experimental Approach

A test chamber was designed and fabricated to study flame spreading and combustion inside the stick perforation, and mechanical deformation of the propellant grain under dynamic loading. Figure 4 is a schematic drawing of the windowed test rig. A long (60 cm) single-stick propellant has been used in the test chamber.

The test chamber has the capability to measure both transient pressures inside the perforation at several axial locations and pressures outside the stick propellant. The chamber has two long windows through which the phenomena of flame spreading, combustion, and fracture can be observed. In the external region of the stick propellant, the initial pressure can be set at a desirable level by using compressed nitrogen gas, or the chamber can be filled completely with water to prolong the propellant fracture event. The internal perforation of the stick propellant is pressurized using hot combustion gases generated from a driving motor. The data-acquisition system contains a transient waveform recorder to store the pressure-time traces during dynamic pressurization. The time of grain

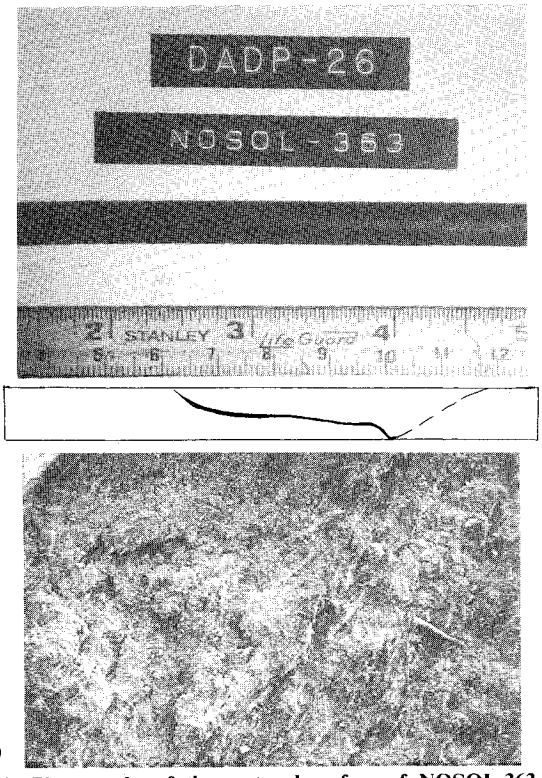

Fig. 6 Photographs of the ruptured surface of NOSOL-363 stick propellant at low pressurization rates: a) photograph of recovered grain with shattered pieces, b) sketch of ruptured grain; and c) SEM photograph of the ruptured surface.

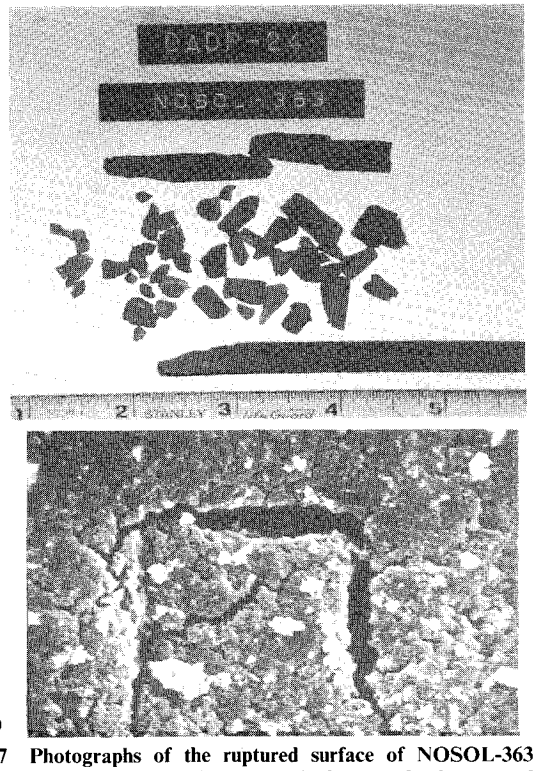

Fig. 7 Photographs of the ruptured surface of NOSOL-363 stick propellant at high pressuration rates: a) photograph of recovered grain with shattered pieces; and b) SEM photograph of the ruptured surface showing the existence of microcracks.

fracture, as well as the critical pressure differential across the propellant web, was determined from the traces and from high-speed movie films. Both high-speed movie and video cameras were used to obtain records of flame spreading, combustion, and grain fracture.

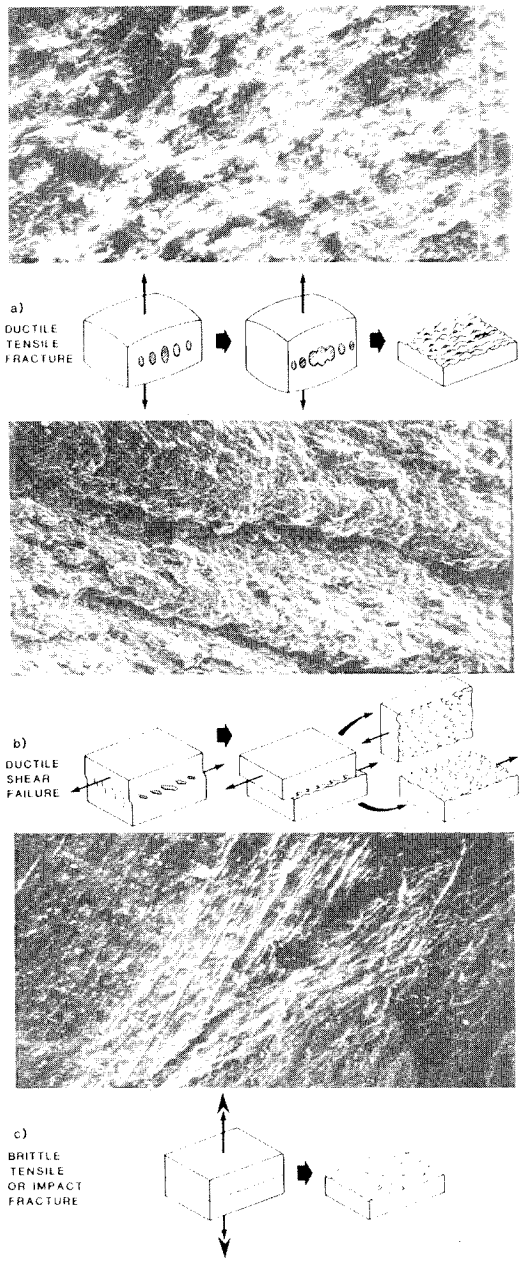

Fig. 8 Ductile-tensile, ductile-shear, and brittle-cleavage phenomena shown on the ruptured surface of NOSOL-363 stick propellant.

Discussion of Results

Numerous tests were conducted using the test chamber previously described. A typical set of pressure-time traces (DADP-18) is shown in Fig. 5. Pressure history at several locations of the propellant was recorded. Detailed physical interpretation of the event is given in the figure, from which the occurrence of propellant grain rupture can be determined.

The microstructure of ruptured surfaces of recovered grains was observed using a scanning electron microscope (SEM). Figures 6a and 6b show recovered NOSOL-363 stick-propellant grains with ruptured surfaces as curved slits. An SEM picture of the fractured surface at a relatively low pressurization rate of 2.35 GPa/s is shown in Fig. 6c. Figures 7a and 7b show the recovered shattered grains for the same propellant under a higher dynamic fracture condition ($\partial P/\partial = 25.28$ GPa/s). It is evident from these photographs that the surface of the shattered pieces contains many microcracks, which are the result of very rapid stress loading. Figures 8a–8c show a set of microstructures from different recovered grains under various test conditions. Propellant grain fractured by ductile tensile, ductile shear, and brittle cleavage, respectively, can also be

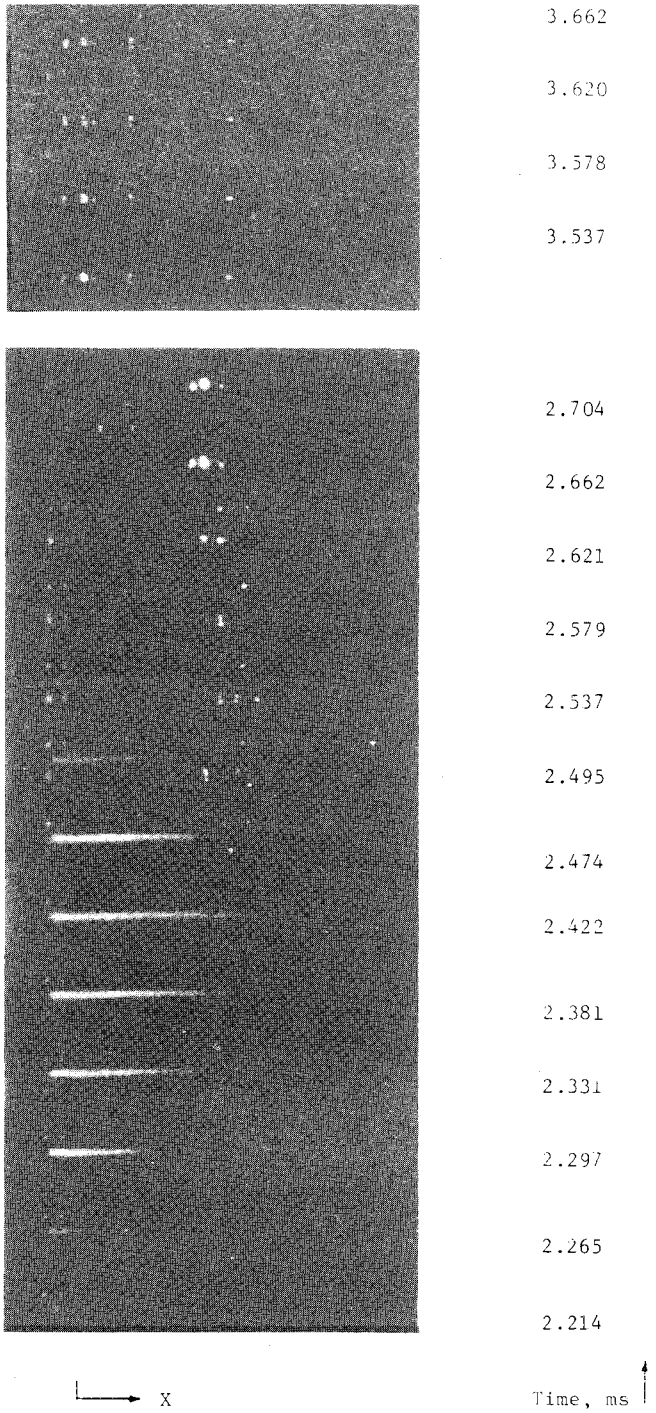

Fig. 9 High-speed pictures showing flame spreading, combustion, and fracture event of a test firing (DADP-26).

observed here; thus, propellant grain fracture could be caused by several factors, depending upon pressurization rate, grain ignition, and combustion conditions in each test.

In order to observe the interaction of flame spreading, combustion, and fracture of stick propellants, high-speed motion pictures were taken during the test using Hycam or Spin Physics (SP-2000) high-speed movie and video cameras. Water was used in the external region to delay the rupture process and observe more clearly the locations of grain rupture. Deformation was not restricted to the center portion of the propellant, and the propellant was photographed only through the first-window portion. As can be seen from Fig. 9 (test no. DADP-26), the propellant was first ignited in the head-end region at time $t = 2.214$ ms, and the flame front propagated into the aft-end region. At $t = 2.454$ ms, the propellant grain ruptured, causing a decrease in the internal

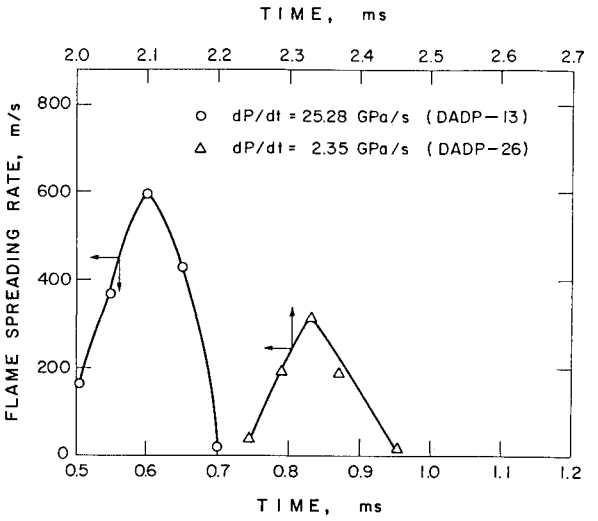

Fig. 10 Flame-spreading rates under different pressurization rates.

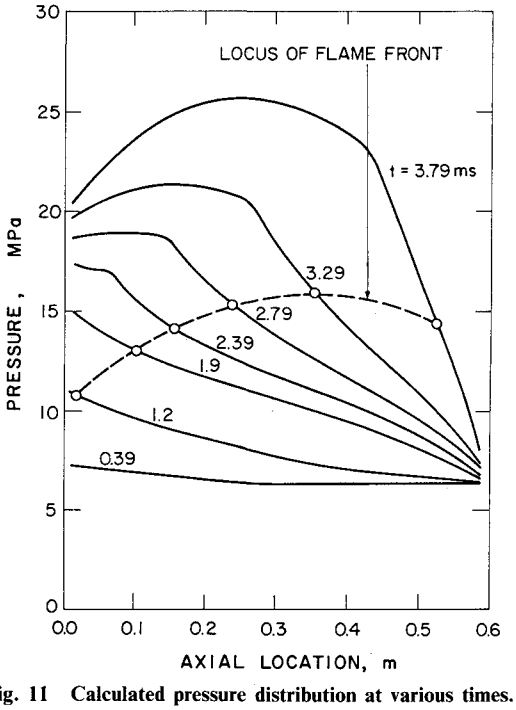

Fig. 11 Calculated pressure distribution at various times.

perforation region pressure, retarded flame spreading, and drastic reduction of flame brightness. At $t = 2.621$ ms, some bright spots were observed, indicating the locations where propellant grain fractured initially. This can be compared with the recovered grain shown in Fig. 6a. After $t = 3.662$ ms, the flame was extinguished by the surrounding water. Based on the pressure-time traces and the high-speed movie films, flame spreading, combustion, and grain-rupture processes of the single-perforated stick propellant can be determined fully. The deformation of propellant grain before rupture was too small to be visible. However, deformation distributions were calculated from the theoretical prediction.

The instantaneous location of the flame front can be determined from the recorded films. The deduced flame-spreading rates corresponding to the flame-front trajectories under different pressurization rates are plotted in Fig. 10. It can be seen that higher pressurization rates produce faster flame-spreading rates.

Theoretical calculation for simulating a typical test (DADP-18) before propellant grain rupture was conducted. The calculated pressure, velocity, and temperature distributions at various times are shown in Figs. 11, 12, and 13,

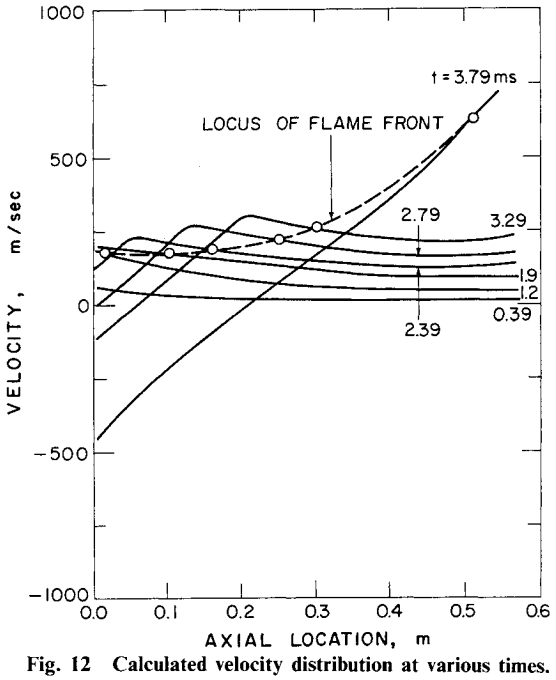

Fig. 12 Calculated velocity distribution at various times.

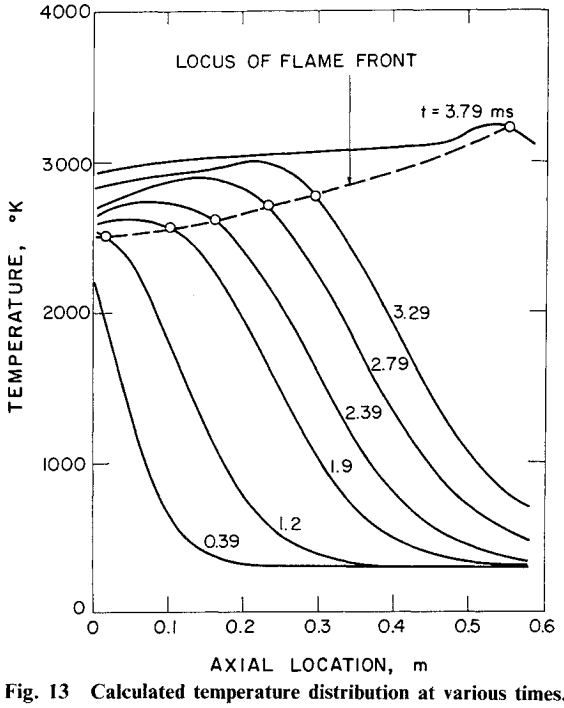

Fig. 13 Calculated temperature distribution at various times.

respectively. The flame-front trajectory is also superimposed on these plots. In Fig. 11, pressure distribution along the axial location decreases monotonically before $t = 1.9$ ms. At times greater than 2.39 ms, a peak pressure with an increase in amplitude develops inside the perforation region. It can be seen that the pressure peak moves downstream as time increases; this is caused by gas accumulation behind the ignition front.

From the predicted velocity distributions at various times (see Fig. 12), it can be seen that at the initial period, the velocity decreases monotonically along the axial location. As the propellant is burned continuously ($t > 2.39$ ms), the peak of the velocity distribution moves downstream because of the local pressure gradient that exists inside the perforation region. At a later time ($t = 2.79$ ms), the combustion gas in the upstream may flow in the reverse direction because of gas flow in the outward directions from the high-pressure region.

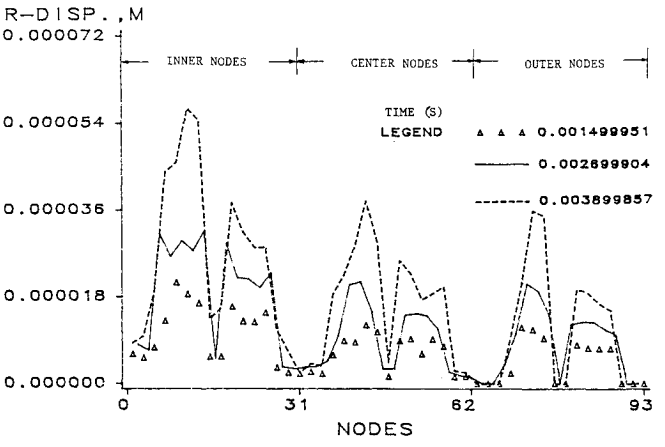

Fig. 14 Calculated radial displacement distribution at various times.

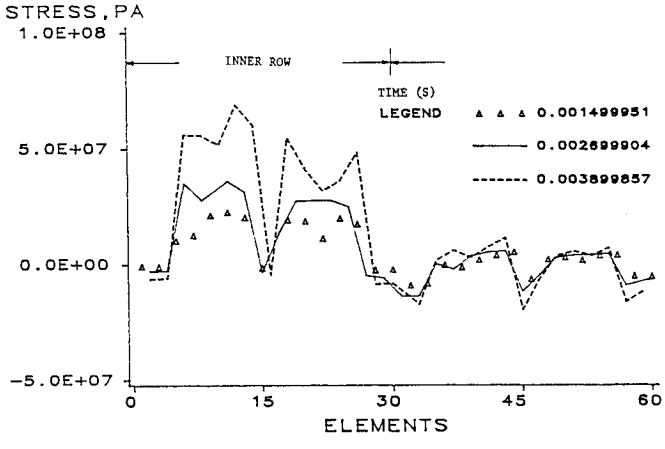

Fig. 15 Calculated stress distribution at various times.

Calculated temperature distributions at various times are shown in Fig. 13. One can see that during the initial time period ($t = 0.39$ ms), a steep temperature gradient is present. This is mainly because the initial increase of the temperature inside the perforation is the result of hot-gas penetration. Since the gas velocity in the downstream is nearly zero during this period, the temperature in the downstream region is also equal to the initial temperature of the gas. As the propellant starts to burn, the temperature inside the perforation region begins to increase and is dominated by the flame temperature of the propellant. In certain downstream locations, the gas temperature is slightly higher than the adiabatic flame temperature of 2958 K; this is due to the effects of gas accumulation and compression before the diaphragm ruptures.

Figure 14 shows the radial-displacement distributions for each row of finite elements along the axial direction at three different times. The web thickness is divided into two rows of finite elements. Three node surfaces bound these elements, each surface containing 31 nodes. Calculated deformations are small compared to the original web thickness. Displacements for the outer row are restricted at three propellant sample-holder locations; therefore, displacement distributions are not uniform. As evident from these curves, the maximum deformation occurs near the center of the first window location.

The calculated stress distribution for each element of the propellant grain is shown in Fig. 15. At $t = 3.8$ ms, the stress at the upstream of the inner element is extremely large. It is expected that propellant grain will rupture near the large stress region; this is very close to the observed rupture location in the high-speed movie films.

Figure 16 presents a comparison of the predicted pressure-time trace at the upstream location with measured data from the test firing. It is evident that they are in good agreement;

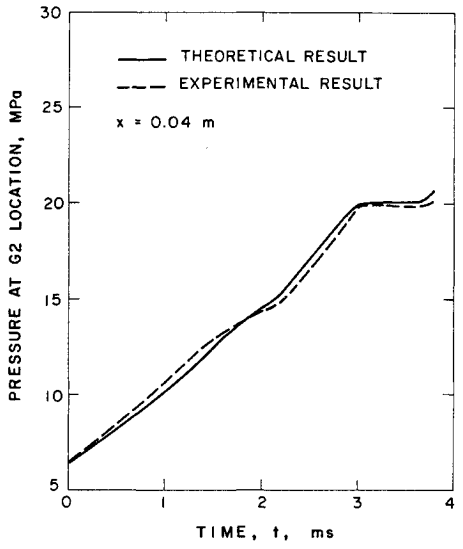

Fig. 16 Comparison of calculated and measured pressure-time traces at upstream locations (pressure gage G2).

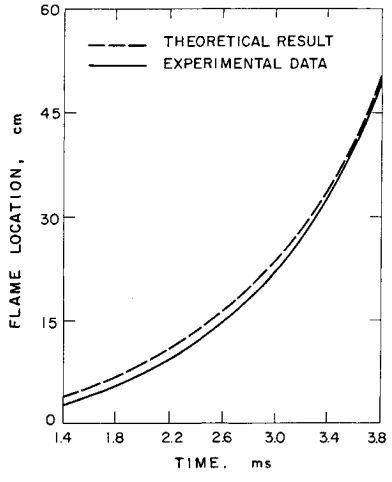

Fig. 17 Comparison of calculated and measured flame-front locations.

the maximum deviation for the predicted value from the test result is about 10%.

Comparison of predicted and measured ignition-front locations is shown in Fig. 17. It can be seen that the model also predicts the trend of the ignition front quite well. Disagreement of these two results may stem from the different criteria used in theory and experiment to determine the flame-front location. In the theoretical calculation, the ignition front is determined as the propellant surface temperature reaches the ignition temperature of 600 K. In the actual film, however, the flame front can be observed only when the gas temperature is high enough to be visible, following which the curve-fitting scheme is used to determine the flame-front locations.

Summary and Conclusions

Some of the major observations and results obtained from this study are summarized as follows:

1) Recovered test samples show that for low pressurization rates, the grain fractures with one or more longitudinal slits; but at very rapid pressurization rates, the propellant shatters into many pieces. This is important since fragments of the shattered propellant generate a significantly higher total burning surface area, which in turn leads to enhanced burning of the propellant.

2) From SEM photographs, fractured surfaces of shattered propellant pieces show the existence of numerous microcracks. Microcracks are absent in the case of low pressurization rate tests.

3) Ignition is earlier and flame spreading is faster for higher pressurization rate conditions.

4) A theoretical model has been developed to analyze the interaction between combustion processes and grain deformation inside the perforation region of single-perforated stick propellants before propellant rupture. Calculated temperature, pressure, velocity, grain deformation, stress distributions, etc., along the flow direction aid in the physical interpretation of the coupled phenomena of combustion and structural mechanics.

5) Comparison of the predicted pressure-time trace with the measured data from test firing shows them to be in good agreement. Based on this agreement, the theoretical model has been further validated to simulate the present problem.

Acknowledgments

This research work represents a part of the results obtained under Contract DAAK 29-83-K-0081, sponsored by the Engineering Science Division, Army Research Office, Research Triangle Park, North Carolina, under the management of Dr. David M. Mann. The authors wish to thank Dr. Mann and Mr. F. W. Robbins of Ballistics Research Laboratory for their support. The assistance of Mr. T. Snyder and Mr. R. Salizzoni on a number of test firings is also appreciated. Acknowledgment is extended to Ms. Z. E. Beisinger of Sandia National Laboratory for supplying the original version of HONDO-II for modification and incorporation into the overall computer code.

References

[1]Robbins, F. W. and Horst, A. W., "Slotted Stick-Propellant Study," *Proceedings of the 20th JANNAF Combustion Meeting*, CPIA Publication 383, Vol. I, Oct. 1983, pp. 377–386.

[2]Robbins, F. W. and Horst, A. W., "A Simple Theoretical Analysis and Experimental Investigation of Burning Processes for Stick Propellant," *Proceedings of the 18th JANNAF Combustion Meeting*, CPIA Publication 347, Vol. II, 1981, pp. 25–34.

[3]Minor, T. C., "Ignition Phenomena in Combustible-Cased Stick Propellant Charges," *Proceedings of the 19th JANNAF Combustion Meeting*, CPIA Publication 366, Vol. I, 1982, pp. 555–567.

[4]Robbins, F. W. and Horst, A. W., "Continued Study of Stick-Propellant Combustion Processes," U.S. Army Ballistic Research Lab., Aberdeen Proving Ground, MD, Rept. ARBRL-MR-03296, July 1983.

[5]Chiu, D., Grabovsky, A., and Downs, D., "Closed-Vessel Combustion Studies of Stick Propellants," *Proceedings of the 20th JANNAF Combustion Meeting*, CPIA Publication 383, Vol. I, 1983, pp. 393–402.

[6]Minor, T., "Mitigation of Ignition-Induced, Two-Phase Flow Dynamics in Guns through the Use of Stick Propellants," U.S. Army Ballistic Research Lab., Aberdeen Proving Grounds, MD, Rept. ARBRL-TR-02508, Aug. 1983.

[7]Athavale, M. M., Hsieh, K. C., Hsieh, W. H., Char, J. M., and Kuo, K. K., "Interaction of Flame-Spreading, Combustion, and Fracture of Single-Perforated Stick Propellants," *Dynamics of Explosion,* AIAA Progress Series, Vol. 105, AIAA, New York, Sept. 1986, pp. 267–290.

[8]Robbins, F. W., Kudzal, J. A., McWilliams, J. A., and Gough, P. S., "Experimental Determination of Stick Charge Flow Resistance," *Proceedings of the 17th JANNAF Combustion Meeting*, CPIA Publication 329, Vol. II, 1980, pp. 97–118.

[9]Gough, P. S., "Continuous Modeling of Stick Charge Combustion," *Proceedings of the 20th JANNAF Combustion Meeting*, CPIA Publication 383, Vol. I, 1983, pp. 351–363.

[10]Gough, P. S., "Modeling of Rigidized Gun Propelling Charges," U.S. Army Ballistic Research Lab., Aberdeen Proving Ground, MD, Rept. ARBRL-CR-00518, 1983.

[11]Horst, A. W., Robbins, F. W., and Gough, P. S., "Multidimensional, Multiphase Flow Analysis of Flame Spreading in a Stick-Propellant Charge," *Proceedings of the 20th JANNAF Combustion Meeting*, CPIA Publication 383, Vol. I, 1983, pp. 365–386.

[12]Key, S. W., Beisinger, Z. E., and Krieg, R. D., "HONDO-II—A Finite-Element Computer Program for the Large Deformation Dynamics of Axisymmetric Solids," Sandia National Lab., Albuquerque, NM, Rept. SAND 78-0422, 1978.